ACS NANO
Cite This: ACS Nano XXXX, XXX, XXX−XXX
www.acsnano.org

ARTICLE

A Hybridized Triboelectric−Electromagnetic Water Wave Energy Harvester Based on a Magnetic Sphere

Zhiyi Wu,[†,‡,⊥] Hengyu Guo,[‡,⊥] Wenbo Ding,[‡,⊥] Yi-Cheng Wang,[§] Lei Zhang,[‡] and Zhong Lin Wang*[,†,‡]

[†]Beijing Institute of Nanoenergy and Nanosystems, Chinese Academy of Sciences, Beijing 100083, China
[‡]School of Materials Science and Engineering, Georgia Institute of Technology, Atlanta, Georgia 30332-0245, United States
[§]Department of Food Science and Human Nutrition, University of Illinois at Urbana−Champaign, Urbana, Illinois 61801, United States

Supporting Information

ABSTRACT: **Blue energy harvested from ocean waves is an important and promising renewable energy source for sustainable development of our society. Triboelectric nanogenerators (TENGs) and electromagnetic energy harvesters (EMGs) both are considered promising approaches for harvesting blue energy. In this work, a hybridized triboelectric−electromagnetic water wave energy harvester (WWEH) based on a magnetic sphere is presented. A freely rolling magnetic sphere senses the water motion to drive the friction object sliding on a solid surface for TENG back and forth. At the same time, two coils transform the motion of the magnetic sphere into electricity according to the electromagnetic induction effect. For harvesting the blue energy from any direction, the electrodes of the TENG are specified as the Tai Chi shape, the effective of which is analyzed and demonstrated. Based on a series of experimental comparisons, the two friction layers and the two coils are specified to be connected in parallel and in series, respectively. A paper-based supercapacitor of ∼1 mF is fabricated to store the generated energy. The WWEH is placed on a buoy to test in Lake Lanier. During 162 s, the supercapacitor can be charged to 1.84 V, the electric energy storage in it is about 1.64 mJ. This work demonstrates that the WWEH can be successfully used for driving distributed, self-powered sensors for environmental monitoring.**

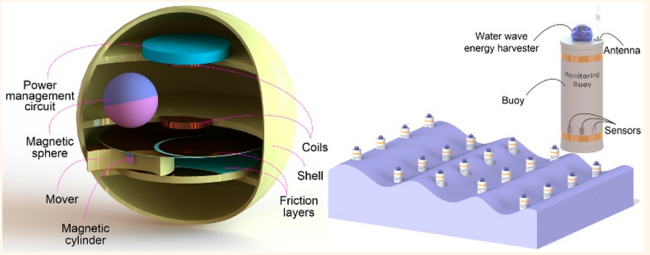

KEYWORDS: *blue energy, triboelectric nanogenerator, electromagnetic generator, magnetic sphere, supercapacitor*

To meet the rapidly increasing global energy demand, developing renewable and clean energy has been a focused goal for the world.[1−3] Nature provides three sources of energy for free: sunlight, air, and gravity.[4] With the technological progress in solar cells and wind turbines, solar and wind power are increasingly exploited and have been successfully commercialized. Oceans cover about 70% of Earth's surface. Water wave energy is independent of seasonality, weather, and day and night. Although having been explored for decades, large-scale harvesting of blue energy still lacks economical technologies.[5,6] Current approaches are entirely based on the principle of electromagnetic induction, through complex mechanical structures or hydraulics to catch water wave energy and convert it into linear reciprocal motion or rotary motion for driving an electromagnetic generator (EMG).[7−10] However, these designs are complicated, heavy, and costly. These disadvantages limit them to be used for large-scale energy harvesting.

Triboelectric nanogenerators (TENGs) based on triboelectrification and electrostatic induction have the merits of large design flexibility, simple structure, abundant choice of materials, and low cost.[11,12] These features render the TENG to be a viable technology to harvest water wave energy.[4,13−31] Since spherical TENGs with a spherical shape or some spherical friction driven structures can easily respond to excitations from any direction, they are the typical structures for harvesting water wave energy.[4,14−19] For enhancing their output performance, the friction contact forms have evolved from point contact to surface contact. Recently, some researchers have demonstrated that hybridized triboelectric−electromagnetic water wave energy harvesters also can be a

Received: November 29, 2018
Accepted: January 25, 2019
Published: January 25, 2019

DOI: 10.1021/acsnano.8b09088
ACS Nano XXXX, XXX, XXX−XXX

good choice for blue energy.[20−24] The performance of the hybridized triboelectric−electromagnetic design also has been demonstrated in some self-powered sensors.[32−36] The driven structures of the hybridized triboelectric−electromagnetic water wave energy harvesters are usually based on a rotor or a sliding rail, which are usually large in size. Hence, introducing the spherical friction driven structures into the hybrid triboelectric−electromagnetic water wave energy harvesters would certainly be a valuable method to optimize the performance of the TENGs for blue energy. In addition, a permanent magnet has been successfully used to drive a TENG-based multifunctional motion sensor.[37]

In this paper, a hybrid triboelectric−electromagnetic water wave energy harvester (WWEH) based on a magnetic sphere is presented, which is capable of capturing the water wave energy from any orientation. The WWEH consists of a TENG module, an electromagnetic generator (EMG) module, a power management circuit, and a spherical acrylic shell. The TENG module is formed by placing a mover between two friction layers. The mover is an acrylic plate embedded with a magnetic cylinder and coated with copper films. The electrode of the friction layer is specified as the Tai Chi shape to ensure the TENG module can have a good output performance, which will not be limited by the mover's motion direction. The EMG module is formed by placing a magnetic sphere between two self-adhesive coils. During the motion of the magnetic sphere excited by the wave, it not only provides a variable magnetic field to the coils but also drives the mover sliding on the friction layers under the magnetic attraction force. A paper-based supercapacitor (P-SC) has been used to construct the power management circuit. The performance of the TENG module, the EMG module, and the P-SC are studied, and the connections of the TENG and EMG modules are also investigated. The WWEH driven by hand can be directly used to light a white LED, even in a bright environment. Based on this, the WWEH was placed on a buoy and tested in Lake Lanier to demonstrate its effectiveness for harvesting water wave energy.

RESULTS AND DISCUSSION

The structure diagram of the hybridized triboelectric−electromagnetic water wave energy harvester and its entity are demonstrated in Figure 1a,b, and Figure S1. The spherical cavity formed by an acrylic shell is divided into four zones by three acrylic discs, which are used for the power management circuit, the EMG module, and the TENG module from the top to the bottom. Two coils are embedded into two acrylic discs, between which the magnetic sphere (NdFeB, N38) is placed. Two friction layers are attached on two acrylic discs, the space between which is used as the movement area for the mover. A magnetic cylinder (NdFeB, N38) which can be attracted by the magnetic sphere is embedded in the mover. The size diagram of the WWEH is shown in Figure S2. The volume of the WWEH is about 523.60 cm^3 with a diameter of 100 mm. The inner diameter, outer diameter, and height of the coil (self-adhesive coil, wire diameter 0.15 mm, turns 900, and resistance 43.8 Ω) are 7.5 mm, 25 mm, and 3 mm, respectively. The diameter of the magnetic sphere and the diameter and height of the magnetic cylinder are 25 mm, 5 mm, and 6 mm, respectively. The diameter and height of the mover are 40 mm and 9 mm, respectively. The friction layer is constituted of a polytetrafluoroethylene (PTFE) plate adhered to two copper electrodes with Tai Chi shape, as shown in Figure 1c and

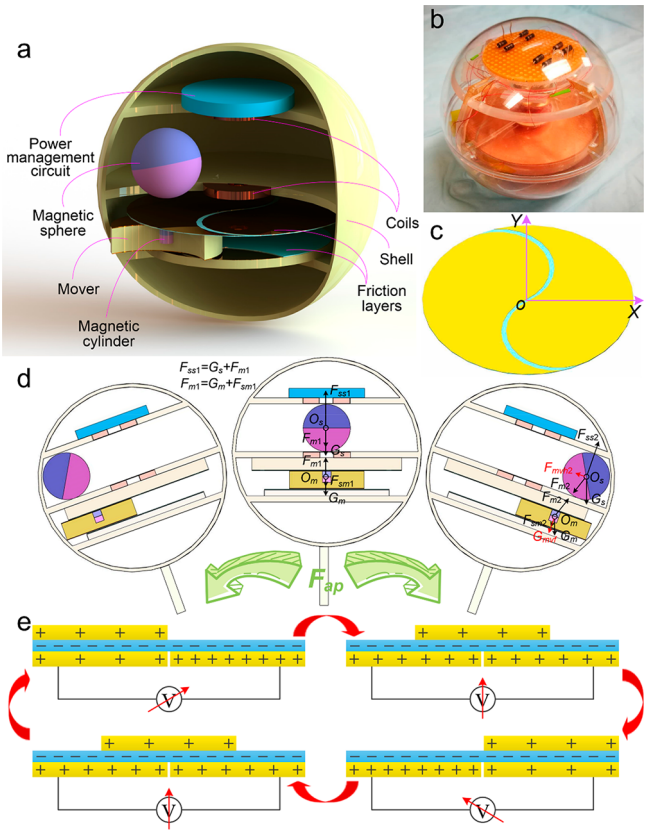

Figure 1. Structure and illustration of the working principle of the hybridized triboelectric−electromagnetic water wave energy harvester. (a) Schematic diagram of the WWEH. (b) Photograph of the WWEH. (c) Schematic diagram of the friction electrodes with Tai Chi shape. (d) Mechanics analysis diagram of the WWEH. (e) Schematic illustration of the working principle of the WWEH to produce electricity.

Figure S2b. The width of a gap between the electrodes is 1 mm. The Tai Chi shape is specified to let the TENG module can harvest the excitations from any orientation. As the core component of the WWEH, the magnetic sphere through response to the water wave motion drives the EMG module by the electromagnetic induction principle and the mover by magnetic attractive force with the magnetic cylinder. And then according to the triboelectrification and electrostatic induction, the mover can drive the TENG module to produce electricity. In order to enhance the movement ranges of the magnetic sphere, the WWEH is usually placed on some flotation device, such as buoys, spars, and so on, to swing with the water wave. The mechanics analysis diagram of the magnetic system is illustrated in Figure 1d. When there is no excitation, the magnetic sphere and the magnetic cylinder will always keep in a balanced place, just like the center place. Under this condition, the gravities (G_s and G_m), the magnetic attraction force between them, F_{m1}, and the supporting forces (F_{ss1} and F_{sm1}) are all along the vertical direction ($F_{ss1} = G_s + F_{m1}$ and $F_{m1} = G_m + F_{sm1}$). A larger F_{m1} will increase the demand of driven condition. But a smaller F_{m1} will provide a small F_{sm1}, which will reduce the output performance of TENG module. As shown in Figure S3, the value of F_{m1} is inversely proportional to the distance between the magnetic sphere and the mover. So, through adjusting the distance, a suitable F_{m1} can be specified to ensure the WWEH can be driven easily

DOI: 10.1021/acsnano.8b09088
ACS Nano XXXX, XXX, XXX−XXX

and has a good output performance. The excitations from any orientation except along the vertical direction will apply a force (F_{ap}) to break the balance, which forces the magnetic sphere to pass through two coils. At the same time, the mover will slide on the friction layers driven by the magnetic sphere. When the magnetic sphere and the mover move to the side, the magnetic sphere usually will rotate some angle. And then, the component of the magnetic force (F_{m2}) parallel to the friction player (F_{mvh2}) will help the water wave to pull the magnetic sphere to another side, as does the mover. In these processes, according the electromagnetic induction principle, the continuously open circuit voltages can be produced by the coils. And based on the triboelectrification and electrostatic induction, the open circuit voltages can also be detected on those Tai Chi electrodes, which are schematically displayed in Figure 1e. When the mover slides on the PTFE plate, owing to the different triboelectric polarity of the PTFE and copper coating around the mover, the electrons will transfer from the copper coating to the PTFE plate, rendering them with positive and negative charges in the saturated state, respectively. The charges on their surfaces cannot be conducted away or neutralized in the harvesting process. Hence, the copper coating can be regarded as an equipotential surface. Then based on electrostatic induction, the open circuit voltages of two electrodes will be changed with the movement of the mover.

To obtain a more quantitative understanding about the magnetic field applied by the magnetic sphere and the magnetic cylinder, a finite-element model simulation is performed using Maxwell 14.0. In Figure 2a, when there no excitations and the magnets stay at the center as an example,

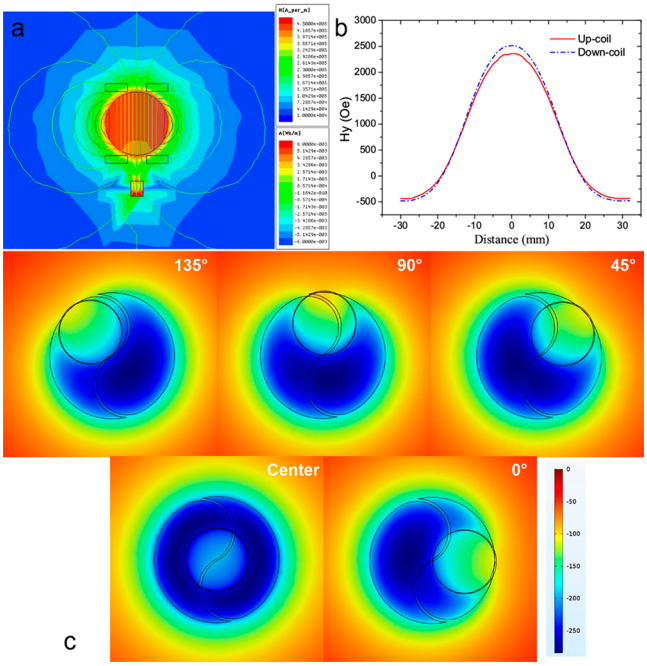

Figure 2. Simulation results of the magnetic sphere and Tai Chi electrodes of the WWEH using Maxwell 14.0 and COMSOL Multiphysics 5.3, respectively. (a) Magnetic distributions of magnetic sphere at the original balance place. (b) The magnetic field applied to the two coils with the magnetic sphere is at different places. (c) Electrostatic potential distributions of the magnetic sphere at the center place, center, 0°, 45°, 90°, and 135°.

the magnetic field and magnetic induction line distributions are center symmetric. In this situation, the magnetic field passing through the coils reaches the maximum value, which has been demonstrated in Figure 2b. When the magnets move from one side to another side, the magnetic fields are applied to the two coils like cosine curves. And under the effect of the magnetic cylinder, the magnetic field applied to the down-coil is a little larger than that of the up-coil. For demonstrating the performance of the Tai Chi electrodes, the electrostatic voltage distributions with the mover moving to different places were simulated by COMSOL Multiphysics 5.3 and are described in Figure 2c. Those distribution patterns of electrostatic potential are calculated by assuming that the mover is regarded as an equipotential body. When the mover is at the center place, the electrostatic potential distribution of the two electrodes is the same. That is to say, there is no electrical potential drop between the electrodes in this situation. Away from this position, an electrical potential difference is produced, especially at 135°. Hence, when the mover slides from one side to another side along any direction, a significant open circuit voltage always can be generated by the TENG module.

An experimental setup composed of a shaker, two electrometers, a data acquisition card, a LabVIEW testing program, and a computer has been established to test the fundamental characteristics of the WWEH, as shown in Figure S4. The WWEH is fixed on the center place of the shaker's worktable. The output of the TENG module is tested by the electrometers and then acquired by the data acquisition card. The output of the EMG module is directly acquired by the data acquisition card. Then, the output signals of the WWEH are processed and exhibited by the LabVIEW testing program. The test process of the experimental setup is recorded in Video S1.

First, the performance of the Tai Chi electrodes has been experimentally verified, as shown in Figure 3a. When the mover swings along any direction, the output voltage of the upper friction layer is at least 72.67 V_{pp} at 30 rpm. When it swings along the 135° direction, the output voltage of the upper friction layer reaches the largest value of 172.95 V_{pp}. The relationship between the output voltage of the upper friction layer and the swing speed in the 135° direction is shown in Figure 3b. With increase of the speed, the output voltage remains nearly the same. In the following, the connecting modes, load, and charging characteristics are tested at 30 rpm in the 135° direction. Figure 3c,d describes the output voltages and output currents of the two friction layers connected in parallel and in series (recorded as TENG-P and TENG-S), respectively. Whether the TENG module is connected in parallel or in series, the output voltage is larger than 120 V_{pp}. The current's peak value of the TENG-P is bigger than that of TENG-S. At the same time, the output voltages and output currents of the two coils connected in parallel and in series (recorded as EMG-P and EMG-S) are plotted in Figure 3e,f, respectively. The output voltage of the EMG-P is smaller than that of the EMG-S, and the output current of the EMG-P is stronger than that of the EMG-S. In order to let the WWEH have good charging characteristics, the TENG and EMG modules are specified to connect in parallel and in series, respectively. The load characteristics of the TENG-P and EMG-S are shown in Figure 4a,b, respectively. The open circuit voltage of the TENG-P is about 180 V_{pp}, which is 100 times larger than that of the EMG-S. Figure 4c describes the

DOI: 10.1021/acsnano.8b09088
ACS Nano XXXX, XXX, XXX−XXX

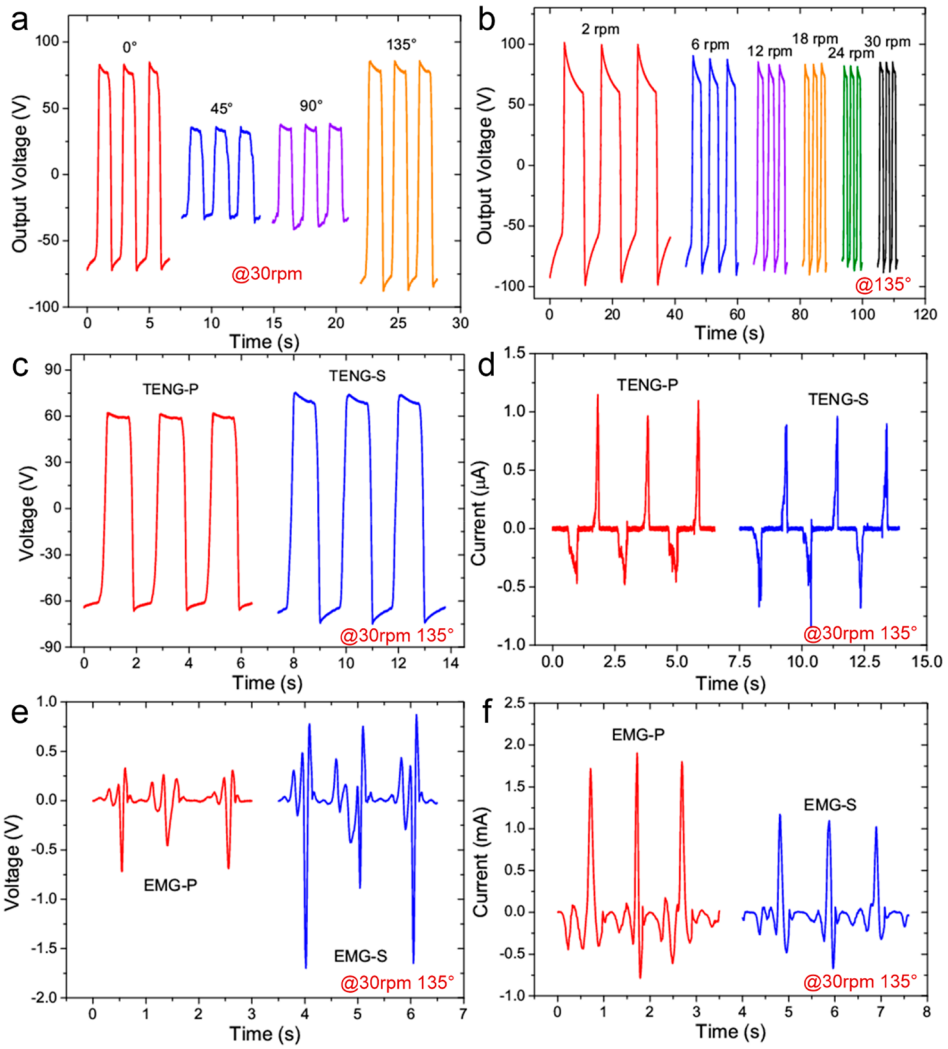

Figure 3. Output performance of the WWEH. (a) Voltage waveforms of the TENG as the magnetic sphere moves along different Tai Chi angles at 30 rpm. (b) Voltage waveforms of the TENG at different rocking speeds at 135°. (c) Voltage waveforms of two TENGs connected in parallel and in series at 30 rpm and 135°. (d) Current waveforms of two TENGs connected in parallel and in series at 30 rpm and 135°. (e) Voltage waveforms of two EMGs connected in parallel and in series at 30 rpm and 135°. (f) Current waveforms of two EMGs connected in parallel and in series with 30 rpm and 135°, respectively.

charging curves of the TENG-P and EMG-S for an electrolytic capacitor of 10 μF. The EMG-S can charge the capacitor to the largest value very rapidly, but the largest value is much smaller than that of the TENG-P. These results show that the large output current provides a fast charging speed to the EMG and the high output voltage lets the TENG have persistent charging ability. Finally, two different rectifier bridges are designed to match with the TENG-P and EMG-S, the connecting modes between which are tested and shown in Figure 4d. Compared with the EMG-S and TENG-P connected in parallel, the EMG-S and TENG-P connected in series can also charge the capacitor to a large value in a very short time, which is about 1 V in this place, and the capacitor can be continuously charged to the largest value. That is to say, the EMG-S and TENG-P connected in series have both the charging advantages of the EMG-S and TENG-P. Hence, the EMG-S and TENG-P connected in series are undoubtedly the best choice. For directly exhibiting the performance of the WWEH, driven by hand, it is used to power a white LED. As shown in Figure 4e, the LED is very bright in the dark environment. And even in the bright environment, the lighting of the LED is also very clearly distinguishable, just like a white speckle, as shown in Figure 4f. The testing process of this can be viewed in Video S2. Moreover, because the acrylic ball is fragile and the thickness of it is only 1 mm, it will be prone to cracks after longtime work, which has been exposed in Figure 4f. So, rubber as an elastic material is a sensible substitute for the acrylic.

According to the fabrication process reported in ref 38, a paper-based supercapacitor is fabricated for electric energy storage, as shown in Figure 5a. For P-SC fabrication, a conductive Au layer is deposited on the surface of a sandpaper by physical vapor deposition before graphite coating as the active material. Figure S5 and Figure 5b show the cross-section and top views of the graphite-based electrode. The properties of the P-SC are evaluated by cyclic voltammetry (CV) and galvanostatic charging/discharging (CD) techniques. Figure 5c shows that with the increase of the scan rate, the rectangular shape of the CV curves does not significantly change, which indicates the good capacitive behavior and high rate charging/discharging ability of the P-SC. CD curves of the P-SC under various current densities are presented in Figure 5b. There is

DOI: 10.1021/acsnano.8b09088
ACS Nano XXXX, XXX, XXX−XXX

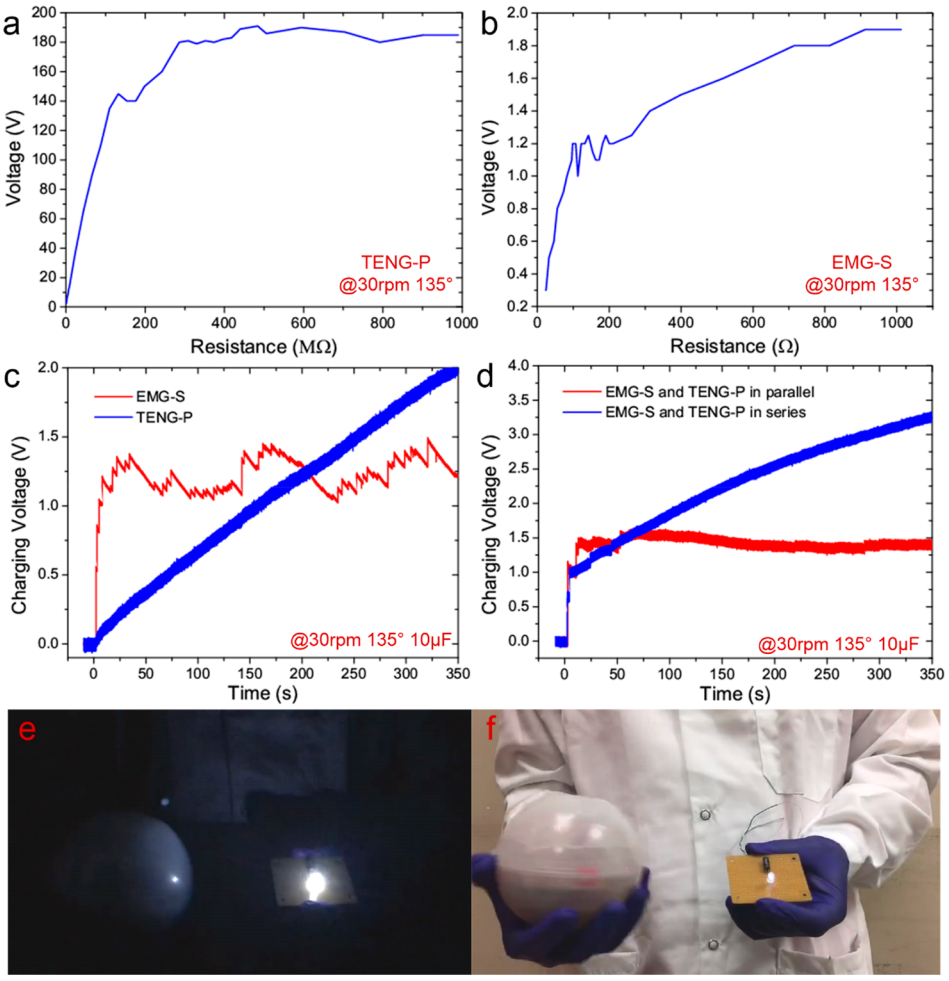

Figure 4. Load, charging characteristics, and hand driven application of the WWEH. (a) Load characteristics of the TENG-P at 30 rpm and 135°. (b) Load characteristics of the EMG-S at 30 rpm and 135°. (c) Charging characteristics of the TENG-P and EMG-S at 30 rpm, 135°, and 10 μF. (d) Charging characteristics of the TENG-P and EMG-S connected in parallel and in series at 30 rpm, 135°, and 10 μF. (e, f) The WWEH driven by hand to power a white LED in a dark and bright environment, respectively.

no obvious I_R-drop observed even at a high discharging rate (100 μA/cm^2), which indicates the outstanding capacitance behavior and excellent conductivity of the graphite electrode. This has been proven by electrochemical impedance spectroscopy shown in Figure S6a. The specific surface capacitance calculated from the CV curve at the corresponding scan rates is shown in Figure S6b. The specific capacitance is found to decrease with increasing scan rate since the incomplete charging/discharging of the electrode material is limited by ionic diffusion. A specific surface capacitance of ~2 mF/cm^2 can be achieved at a scan rate of 5 mV/s. Finally, several P-SC units (nos. 1−4) have been integrated into assemblies both in series and in parallel connection to meet specific energy needs for practical applications, the performances of which are shown in Figure S7. All these results show that the tunable adaptability and reliable scalability of the P-SC to practical applications. Hence, in order to provide a large working voltage, four P-SC units with size of 2 cm^2 are specified to connect in series, the capacitance of which is ~1 mF.

The performance of the WWEH has been verified in Lake Lanier, which is a reservoir in the northern portion of the U.S. state of Georgia. Video S3 indicates that a buoy rocks wildly on the lake under the force of the water wave. After being coated with silicone for water-proofing, the WWEH is fixed on a homemade buoy, the entity of which is shown in Figure S8. Figure S9 presents the test environment of the WWEH. Some soft strings are used to tie the buoy to avoid it being pushed to the bank by the water waves, while not restricting its motion. Energy storage in the S-PC is monitored by a multimeter. The whole lake testing lasted about 200 s, as recorded in Video S4. Because of the randomness of the water waves, their amplitude could not always be kept the same. This directly affected the charging speed, which is presented in Figure 5e. During 162 s, the P-SC was charged to 1.84 V. So, the energy storage in it can be calculated as 1.69 mJ.[39] As shown in Figure 5f, the WWEH-based buoy is used to construct some self-powered wireless sensor networks for environmental monitoring, such as temperature, pH, oxygen level, and so on. Because of the magnetic sphere in the assembly, the distances between the WWEH-based buoys should be large enough to avoid the influence of magnetic attractive forces between the magnetic spheres. Through utilizing a temperature switch as a control unit, a self-powered wireless water temperature alarm system was built, a schematic diagram of which is provided in Figure 5g. The water wave energy harvested by the WWEH is saved in an energy storage unit. When the water temperature is higher than the trigger threshold of the temperature switch, it will be rapidly closed. Then, a Low Dropout Regulator (LDO) unit

DOI: 10.1021/acsnano.8b09088
ACS Nano XXXX, XXX, XXX−XXX

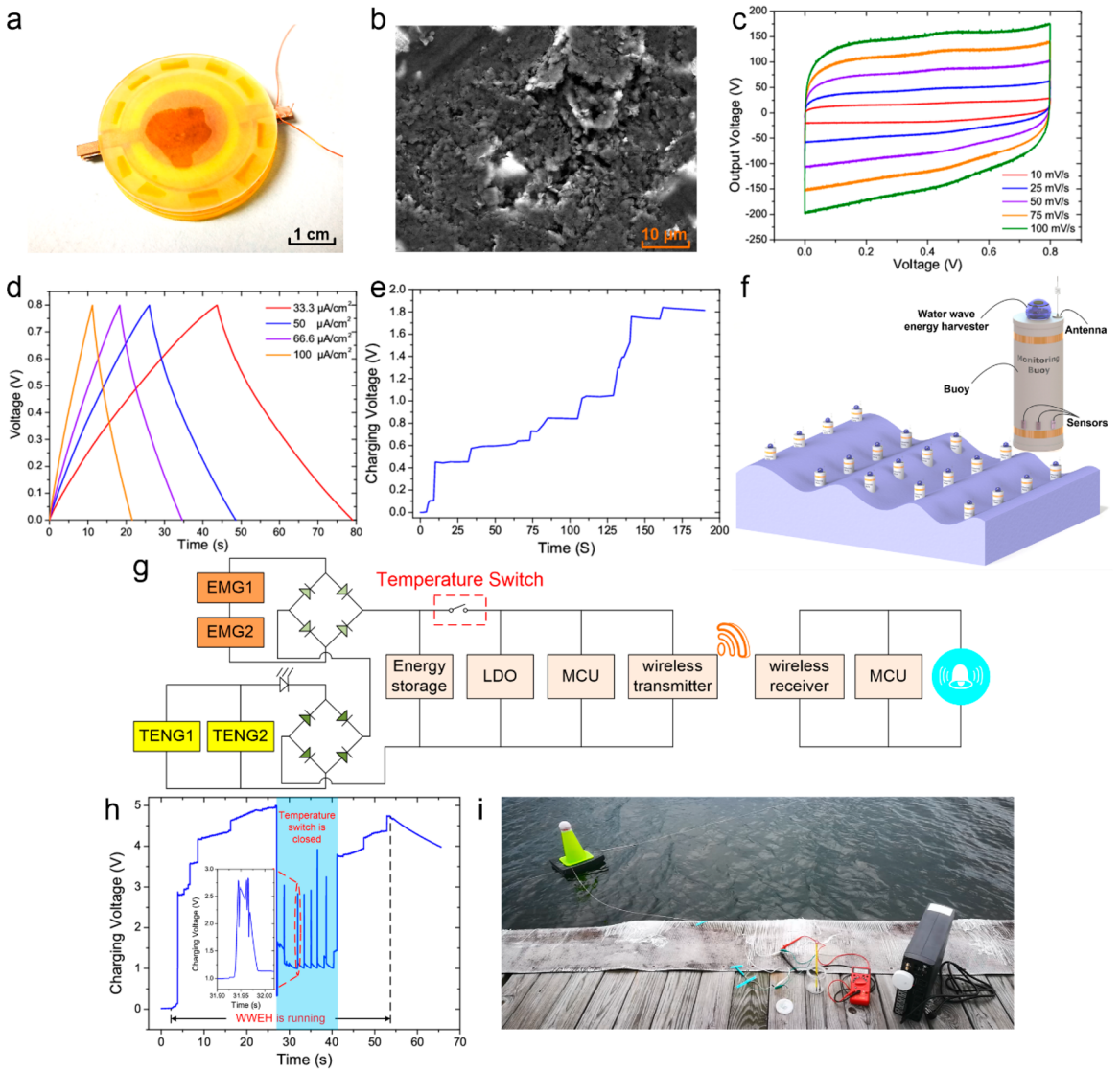

Figure 5. Performance of the P-SC for energy storage and the lake test applications of the WWEH. (a) Photograph of the P-SC. (b) SEM image of the sand paper coated with Au and C in sequence. (c) CV curves of the P-SC under various scanning rates (10−100 mV/s). (d) Galvanostatic charge/discharge curves of the P-SC at different current densities (33.3−100 μA/cm^2). (e) The charging curve of the WWEH placed on a buoy to test in a lake. (f) Schematic illustration of the buoy network based on the WWEH for environmental monitoring. (g) Schematic diagram of a self-powered wireless water temperature alarm system. (h) Typical working waveform of the temperature alarm system. (i) Photograph of the temperature alarm system testing in a lake.

transforms the energy into a stable DC voltage to power the follow-up circuit. A microcontroller unit (MCU) controls the wireless transmitter to send a control command, which will be received by the wireless receiver to help another MCU control a bell ringing. The typical working waveform of the temperature alarm system is plotted in Figure 5h. The operating voltages of the MCU and the wireless receiver are 3.3 V. So, when the temperature switch is closed, a charging voltage larger than 2.75 V makes sure the LDO unit can provide sufficient energy to power the follow-up circuit. This has been demonstrated in the inset figure of Figure 5h. As shown in Figure 5i and Figure S10, the performance of the temperature alarm system is verified in Lake Lanier and recorded in Video S5.

CONCLUSIONS

In summary, to efficiently capture water wave energy, the authors of this paper designed and fabricated a hybridized triboelectric−electromagnetic water wave energy harvester based on a magnetic sphere, which is the core component of the WWEH to response the water wave motion. With the movement of the magnetic sphere, the EMG module according to the electromagnetic induction principle will produce electricity, and the mover under the action of the magnetic attractive force will slide on the friction layers. Then according to the triboelectrification and electrostatic induction, a large output voltage can be detected on the TENG module. To reduce the influence of the water wave excitation orientation, the electrodes of the TENG module are organized into the Tai Chi shape, the performance of which has been analyzed and verified. When the mover swings along any direction, the output voltage is at least 72.67 V_{pp} at 30 rpm. When the mover

DOI: 10.1021/acsnano.8b09088
ACS Nano XXXX, XXX, XXX−XXX

swings along the 135° direction, the output voltage reaches the largest value of 172.95 V_{pp}. Based on a series of experimental comparisons and analysis, the two friction layers of the TENG module and the two coils of the EMG module are connected in parallel and in series, respectively. After being connected with the matching rectifier bridges, the TENG and EMG modules are connected in series to charge an energy storage unit. Because the P-SC has tunable adaptability and reliable scalability to practical applications, a customized P-SC with ~1 mF capacity is used for electric energy storage. Then, after the unit was fixed on a homemade buoy, the performance of the WWEH was verified in Lake Lanier. During 162 s, the P-SC was charged to 1.84 V; the energy storage in it can be calculated as 1.69 mJ. Through increasing the number of the coils, choosing a much stronger magnetic sphere with larger size, enlarging the surface of the friction layer, etc., the performance of the WWEH can be further improved. With to the WWEH-based buoy, some self-powered wireless sensor networks can be constructed to monitor environmental parameters, such as temperature, pH, oxygen level, and so on. Utilizing a temperature switch, a self-powered wireless water temperature alarm system has been built and tested, which confirmed the technical feasibility of the WWEH-based self-powered wireless sensor networks for environmental monitoring.

EXPERIMENTAL SECTION

Fabrication of the Friction Layer. It has been demonstrated that the chemical constitution of the friction material with more fluorine atom can provide a better output performance. The PTFE usually is a good choice. So, the friction layer of the WWEH consists of a PTFE plate and two electrodes which form the Tai Chi shape. A PTFE thin film with 3M very high bond adhesive (McMaster-Carr, thickness 0.002 and 0.0015 in.) was cleaned and cut into a circle with diameter of 79 and 66 mm to make the PTFE plates. A highly conductive copper electrical tape with nonconductive adhesive (McMaster-Carr, thickness 0.0014 and 0.0015 in.) was cleaned and cut into different dimensions shown in Figure S2b (Supporting Information) to make the electrodes. To ensure the electrodes can be accurately fixed on the right places of the PTFE plate, an acrylic mask with thickness of 0.063 in. was made by a laser cutter (PLS6.75, Universal Laser Systems).

Fabrication of the Shell. For monitoring the motion process of the magnetic sphere, the shell of the WWEH is fabricated with clear acrylic. The acrylic ball with diameter of 100 mm and thickness of 1 mm was purchased online. The three acrylic discs with diameters of 79.86, 96.34, and 86.18 mm were made by the laser cutter with a 0.125 in. acrylic plate. The first two discs were engraved with a hollow of diameter 25.2 mm and depth 3 mm in the center for the coils. In the future application, rubber as an elastic material is a sensible substitute for the acrylic.

ASSOCIATED CONTENT

Supporting Information

The Supporting Information is available free of charge on the ACS Publications website at DOI: 10.1021/acsnano.8b09088.

Schematic of the water wave energy harvester, size diagram of the harvester and the friction layer, simulated results of the magnetic attractive force, photograph of an experimental system, SEM image of the graphite-based electrode, performance of the P-SC, photograph of the buoy, photograph of the test environment, and photograph of the water temperature alarm system (PDF)

Experimental setup for fundamental test (MP4)

Proposed harvester driven by hand to power a white LED (MP4)

Typical motion state of a buoy (MP4)

Test of the proposed harvester in a lake environment (MP4)

Test of the temperature alarm system in a lake environment (MP4)

AUTHOR INFORMATION

Corresponding Author

*E-mail: zhong.wang@mse.gatech.edu.

ORCID

Zhong Lin Wang: 0000-0002-5530-0380

Author Contributions

⊥Z.W., H.G., and Y.-C.W. contributed equally to this work.

Notes

The authors declare no competing financial interest.

ACKNOWLEDGMENTS

This research was supported by the Hightower Chair Foundation of Georgia Institute of Technology, the National Natural Science Foundation of China (61503051), the Natural Science Foundation of Chongqing (cstc2017jcyjAX0124), and the Program for Innovation Team Building at Institutions of Higher Education in Chongqing (Grant No. CXTDX201601029). Z.W. thanks the China Scholarship Council for supporting research at Georgia Institute of Technology.

REFERENCES

(1) Schiermeier, Q.; Tollefson, J.; Scully, T.; Witze, A.; Morton, O. Energy Alternatives: Electricity without Carbon. *Nature* **2008**, *454*, 816−823.

(2) Tollefson, J. Blue Energy. *Nature* **2014**, *508*, 302.

(3) Gielen, D.; Boshell, F.; Saygin, D. Climate and Energy Challenges for Materials Science. *Nat. Mater.* **2016**, *15*, 117.

(4) Wang, Z. L. Catch Wave Power in Floating Nets. *Nature* **2017**, *542*, 159.

(5) Salter, S. H. Wave Power. *Nature* **1974**, *249*, 720−724.

(6) Falcão, A. F. d. O. Wave Energy Utilization: A Review of the Technologies. *Renewable Sustainable Energy Rev.* **2010**, *14*, 899−918.

(7) Lagoun, M.; Benalia, A.; Benbouzid, M. H. Ocean Wave Converters: State of the Art and Current Status; In *2010 IEEE International Energy Conference and Exhibition*; IEEE: 2010; pp 636−641.

(8) McCormick, M. E. *Ocean Wave Energy Conversion*; Courier Corporation: 2013.

(9) López, I.; Andreu, J.; Ceballos, S.; de Alegría, I. M.; Kortabarria, I. Review of Wave Energy Technologies and the Necessary Power-Equipment. *Renewable Sustainable Energy Rev.* **2013**, *27*, 413−434.

(10) Falcão, A. F.; Henriques, J. C. Oscillating-Water-Column Wave Energy Converters and Air Turbines: A review. *Renewable Energy* **2016**, *85*, 1391−1424.

(11) Fan, F.-R.; Tian, Z.-Q.; Lin Wang, Z. Flexible Triboelectric Generator. *Nano Energy* **2012**, *1*, 328−334.

(12) Wang, Z. L.; Lin, L.; Chen, J.; Niu, S.; Zi, Y. *Triboelectric Nanogenerators*; Springer: 2016.

(13) Zhu, G.; Su, Y.; Bai, P.; Chen, J.; Jing, Q.; Yang, W.; Wang, Z. L. Harvesting Water Wave Energy by Asymmetric Screening of Electrostatic Charges on a Nanostructured Hydrophobic Thin-Film Surface. *ACS Nano* **2014**, *8*, 6031−6037.

(14) Chen, J.; Yang, J.; Li, Z.; Fan, X.; Zi, Y.; Jing, Q.; Guo, H.; Wen, Z.; Pradel, K. C.; Niu, S.; Wang, Z. L. Networks of Triboelectric Nanogenerators for Harvesting Water Wave Energy: A Potential Approach Toward Blue Energy. *ACS Nano* **2015**, *9*, 3324−3331.

DOI: 10.1021/acsnano.8b09088
ACS Nano XXXX, XXX, XXX−XXX

(15) Wang, X.; Niu, S.; Yin, Y.; Yi, F.; You, Z.; Wang, Z. L. Triboelectric Nanogenerator Based on Fully Enclosed Rolling Spherical Structure for Harvesting Low-Frequency Water Wave Energy. *Adv. Energy Mater.* **2015**, *5*, 1501467.
(16) Jiang, T.; Zhang, L. M.; Chen, X.; Han, C. B.; Tang, W.; Zhang, C.; Xu, L.; Wang, Z. L. Structural Optimization of Triboelectric Nanogenerator for Harvesting Water Wave Energy. *ACS Nano* **2015**, *9*, 12562−12572.
(17) Wang, Z. L.; Jiang, T.; Xu, L. Toward the Blue Energy Dream by Triboelectric Nanogenerator Networks. *Nano Energy* **2017**, *39*, 9−23.
(18) Xu, L.; Jiang, T.; Lin, P.; Shao, J.; He, C.; Zhong, W.; Chen, X.; Wang, Z. L. Coupled Triboelectric Nanogenerator Networks for Efficient Water Wave Energy Harvesting. *ACS Nano* **2018**, *12*, 1849−1858.
(19) Xiao, T. X.; Liang, X.; Jiang, T.; Xu, L.; Shao, J. J.; Nie, J. H.; Bai, Y.; Zhong, W.; Wang, Z. L. Spherical Triboelectric Nanogenerators Based on Spring-Assisted Multilayered Structure for Efficient Water Wave Energy Harvesting. *Adv. Funct. Mater.* **2018**, *28*, 1802634.
(20) Guo, H.; Wen, Z.; Zi, Y.; Yeh, M. H.; Wang, J.; Zhu, L.; Hu, C.; Wang, Z. L. A Water-Proof Triboelectric−Electromagnetic Hybrid Generator for Energy Harvesting in Harsh Environments. *Adv. Energy Mater.* **2016**, *6*, 1501593.
(21) Wen, Z.; Guo, H.; Zi, Y.; Yeh, M.-H.; Wang, X.; Deng, J.; Wang, J.; Li, S.; Hu, C.; Zhu, L.; Wang, Z. L. Harvesting Broad Frequency Band Blue Energy by a Triboelectric−Electromagnetic Hybrid Nanogenerator. *ACS Nano* **2016**, *10*, 6526−6534.
(22) Wang, X.; Wen, Z.; Guo, H.; Wu, C.; He, X.; Lin, L.; Cao, X.; Wang, Z. L. Fully Packaged Blue Energy Harvester by Hybridizing a Rolling Triboelectric Nanogenerator and an Electromagnetic Generator. *ACS Nano* **2016**, *10*, 11369−11376.
(23) Shao, H.; Wen, Z.; Cheng, P.; Sun, N.; Shen, Q.; Zhou, C.; Peng, M.; Yang, Y.; Xie, X.; Sun, X. Multifunctional Power Unit by Hybridizing Contact-Separate Triboelectric Nanogenerator, Electromagnetic Generator and Solar Cell for Harvesting Blue Energy. *Nano Energy* **2017**, *39*, 608−615.
(24) Xie, Y.; Zhang, H.; Yao, G.; Khan, S. A.; Gao, M.; Su, Y.; Yang, W.; Lin, Y. Intelligent Sensing System Based on Hybrid Nanogenerator by Harvesting Multiple Clean Energy. *Adv. Eng. Mater.* **2018**, *20*, 1700886.
(25) Xi, Y.; Guo, H.; Zi, Y.; Li, X.; Wang, J.; Deng, J.; Li, S.; Hu, C.; Cao, X.; Wang, Z. L. Multifunctional TENG for Blue Energy Scavenging and Self-Powered Wind-Speed Sensor. *Adv. Energy Mater.* **2017**, *7*, 1602397.
(26) Jiang, T.; Yao, Y.; Xu, L.; Zhang, L.; Xiao, T.; Wang, Z. L. Spring-Assisted Triboelectric Nanogenerator for Efficiently Harvesting Water Wave Energy. *Nano Energy* **2017**, *31*, 560−567.
(27) Chen, B. D.; Tang, W.; He, C.; Deng, C. R.; Yang, L. J.; Zhu, L. P.; Chen, J.; Shao, J. J.; Liu, L.; Wang, Z. L. Water Wave Energy Harvesting and Self-Powered Liquid-Surface Fluctuation Sensing Based on Bionic-Jellyfish Triboelectric Nanogenerator. *Mater. Today* **2018**, *21*, 88−97.
(28) Kim, D. Y.; Kim, H. S.; Kong, D. S.; Choi, M.; Kim, H. B.; Lee, J.-H.; Murillo, G.; Lee, M.; Kim, S. S.; Jung, J. H. Floating Buoy-Based Triboelectric Nanogenerator for an Effective Vibrational Energy Harvesting from Irregular and Random Water Waves in Wild Sea. *Nano Energy* **2018**, *45*, 247−254.
(29) Li, X.; Tao, J.; Wang, X.; Zhu, J.; Pan, C.; Wang, Z. L. Networks of High Performance Triboelectric Nanogenerators Based on Liquid−Solid Interface Contact Electrification for Harvesting Low-Frequency Blue Energy. *Adv. Energy Mater.* **2018**, *8*, 1800705.
(30) Pan, L.; Wang, J.; Wang, P.; Gao, R.; Wang, Y.-C.; Zhang, X.; Zou, J.-J.; Wang, Z. L. Liquid-FEP-Based U-Tube Triboelectric Nanogenerator for Harvesting Water-Wave Energy. *Nano Res.* **2018**, *11*, 4062−4073.
(31) Zhang, S. L.; Xu, M.; Zhang, C.; Wang, Y.-C.; Zou, H.; He, X.; Wang, Z.; Wang, Z. L. Rationally Designed Sea Snake Structure Based Triboelectric Nanogenerators for Effectively and Efficiently Harvesting Ocean Wave Energy with Minimized Water Screening Effect. *Nano Energy* **2018**, *48*, 421−429.
(32) Askari, H.; Asadi, E.; Saadatnia, Z.; Khajepour, A.; Khamesee, M. B.; Zu, J. A Hybridized Electromagnetic-Triboelectric Self-Powered Sensor for Traffic Monitoring: Concept, Modelling, and Optimization. *Nano Energy* **2017**, *32*, 105−116.
(33) Wang, P.; Liu, R.; Ding, W.; Zhang, P.; Pan, L.; Dai, G.; Zou, H.; Dong, K.; Xu, C.; Wang, Z. L. Complementary Electromagnetic-Triboelectric Active Sensor for Detecting Multiple Mechanical Triggering. *Adv. Funct. Mater.* **2018**, *28*, 1705808.
(34) Askari, H.; Saadatnia, Z.; Asadi, E.; Khajepour, A.; Khamesee, M. B.; Zu, J. A Flexible Hybridized Electromagnetic-Triboelectric Multi-Purpose Self-Powered Sensor. *Nano Energy* **2018**, *45*, 319−329.
(35) Askari, H.; Asadi, E.; Saadatnia, Z.; Khajepour, A.; Khamesee, M. B.; Zu, J. A Flexible Tube-Based Triboelectric-Electromagnetic Sensor for Knee Rehabilitation Assessment. *Sens. Actuators, A* **2018**, *279*, 694−704.
(36) Askari, H.; Hashemi, E.; Khajepour, A.; Khamesee, M. B.; Wang, Z. L. Tire Condition Monitoring and Intelligent Tires Using Nanogenerators Based on Piezoelectric, Electromagnetic, and Triboelectric Effects. *Adv. Mater. Technol.* **2019**, *4*, 1800105.
(37) Wu, Z.; Ding, W.; Dai, Y.; Dong, K.; Wu, C.; Zhang, L.; Lin, Z.; Cheng, J.; Wang, Z. L. Self-Powered Multifunctional Motion Sensor Enabled by Magnetic-Regulated Triboelectric Nanogenerator. *ACS Nano* **2018**, *12*, 5726−5733.
(38) Guo, H.; Yeh, M.-H.; Zi, Y.; Wen, Z.; Chen, J.; Liu, G.; Hu, C.; Wang, Z. L. Ultralight Cut-Paper-Based Self-Charging Power Unit for Self-Powered Portable Electronic and Medical Systems. *ACS Nano* **2017**, *11*, 4475−4482.
(39) Wu, Z.; Wen, Y.; Li, P. A Power Supply of Self-Powered Online Monitoring Systems for Power Cords. *IEEE Trans. Energy Convers.* **2013**, *28*, 921−928.

DOI: 10.1021/acsnano.8b09088
ACS Nano XXXX, XXX, XXX−XXX